nature materials

SUPPLEMENTARY INFORMATION

DOI: 10.1038/NMAT4427

Three-dimensional macroporous nanoelectronic networks as minimally invasive brain probes

Chong Xie, Jia Liu, Tian-Ming Fu, Xiaochuan Dai, Wei Zhou and Charles M. Lieber

This file includes:

Supplementary Methods

Figures S1-S8

Supplementary References

Supplementary Movie Captions

© 2015 Macmillan Publishers Limited. All rights reserved

DOI: 10.1038/NMAT4427

Supplementary Methods

Nanowire Synthesis.

Uniform 30 nm *p*-type single crystal silicon nanowires were synthesized using our reported gold nanocluster-catalyzed vapor-liquid-solid methodology[S1]. In a typical synthesis, the total pressure was 40 torr and the flow rates of SiH_4, diborane (B_2H_6, 100 p.p.m. in H_2), and hydrogen (H_2, Semiconductor Grade), were 2, 2.5 and 60 standard cubic centimetres per minute (SCCM), respectively. The silicon-boron feed-in ratio was 4000:1, and the total nanowire growth time was 30 min.

Macroporous nanoelectronic brain probe fabrication

The macroporous nanoelectronic brain probes were fabricated with key steps as follows: (*i*) photolithography and thermal deposition were used to pattern a 100 nm nickel sacrificial layer, where the nickel served as the final relief layer for the free-standing probe. (*ii*) Photolithography and thermal deposition were used to define the Cr/Pd/Cr (10-20/80/1.5 nm) non-symmetric metal ribbons to generate the strain for global scrolling. Typically, this layer consists of 3-μm wide parallel ribbons. (*iii*) A 300-500 nm layer of SU-8 photoresist was defined by photolithography as the bottom SU-8 passivation layer. Typically, this layer consists of 7-μm wide parallel ribbons. (*iv*) Either nanowire FETs or Pt electrodes were patterned as the voltage sensors (details in the following section). (*v*) Photolithography and thermal deposition were used to define the Cr/Pd/Cr (1.5/80/50-80 nm) double metal ribbons to generate strain for local bend-out from the global cylindrical structure. Typically, this layer consists of 3-μm wide metal interconnect lines. (*vi*) Photolithography and thermal deposition were used to define the non-strained metal contacts, Cr/Au/Cr (1.5/100/1.5 nm), to address each sensor and form interconnections to the input/output pads, which are patterned outside the Ni sacrificial layer. This layer usually consists of 5-μm

© 2015 Macmillan Publishers Limited. All rights reserved

wide metal interconnect lines. (*vii*) Another 300-500 nm thick layer of SU-8 photoresist was defined by photolithography as the top SU-8 passivation. This layer typically has the same pattern as the bottom SU-8 passivation layer in (*iii*).

It should be noted that Pd is a toxic metal and may cause side effect if exposed. In this work the Pd is well protected by the SU8 encapsulation. However, in future long-term applications, other metals, such as Pt or Ti, which are known to make good contact with Si nanowire[S2] and can provide controllable strain[S3], can be used to replace Pd to eliminate possible toxicity.

Nanowire FET sensor patterning.

(a) A 300 to 400 nm layer of SU-8 photoresist was deposited on the fabrication substrate, prebaked (65 °C/2 min; 95 °C/4 min), and then (b) silicon nanowires were aligned on the SU-8 layer by contact printing as described previously[S4]. (c) Photolithography was used to define the nanowire device regions, and after post-baking (65 °C/2 min; 95 °C/2 min), the pattern was developed by SU-8 Developer washed with isopropanol (2 times, 30 s per wash) to remove nanowires outside of the device regions. (d) The new SU-8 pattern was cured at 180 °C/20 min. (e) Nanowire device element contacts were defined by photolithography and Cr/Pd/Cr (1.5/50–80/1.5 nm) metallization.

Metal electrode sensor patterning.

Cr/Pt (1.5/100 nm) electrodes are patterned by photolithography. The electrode size used in this work was 4 μm x 20 μm, with typical impedance of 600 ± 20 kohm at 1 kHz.

© 2015 Macmillan Publishers Limited. All rights reserved

DOI: 10.1038/NMAT4427

Calculation of the bending stiffness for different neural probes.

The mechanical characteristics of the three-layer longitudinal ribbons make the dominant contribution to the probe-tissue interface. The bending stiffness of a single ribbon, K_{1R}, can be estimated as[S5]

$$K_{1R} = E_s\left(\frac{h^3 w_1}{12} - \frac{h_m^3 w_m}{12}\right) + E_m \frac{h_m^3 w_m}{12}$$

where E_s is young's modulus of SU-8, E_m is young's modulus of gold, h is the total thickness of ribbon, h_m is the thickness of metal, w_1 is the total width of ribbon and w_m is the width of metal. When E_s = 2 GPa, E_m = 79 GPa, h = 800 nm, h_m = 100 nm, w_1 = 7 μm, and w_m = 5 μm, K_{1R} = 0.64×10^{-15} N·m^2.

The bending stiffness of another representative component of the probe, the sensor device support arm, K_{1S}, is calculated similarly taking w_1 = 6 μm, w_m = 4 μm. K_{1S} = 0.54×10^{-15} N·m^2.

The bending stiffness of standard silicon probes or planar thin film probes, K_2, can be estimated as[S5]

$$K_2 = E\frac{wh^3}{12}$$

where E is the young's modulus of the probe material, h is the thickness of the probe, and w is the width of the probe. When $E_{silicon}$ = 165 GPa, $h_{silicon}$ = 15 μm, and w = 100 μm, the bending stiffness of a typical silicon probe is K_{2s} = 4.6 x 10^{-8} N·m^2. When $E_{\text{polyimide}}$ = 2 GPa, $h_{\text{polyimide}}$ = 10 μm, and w = 100 μm, the bending stiffness of a typical polyimide probe is K_{2P} = 0.16 x 10^{-10} N·m^2.

The bending stiffness of ultrasmall carbon electrodes, K_3, can be estimated as[S5]

$$K_3 = E_{carbon}\frac{\pi d^4}{64}$$

© 2015 Macmillan Publishers Limited. All rights reserved

Where E_{carbon} is the young's modulus of carbon fiber, d is the diameter of carbon fiber probe. When E_{carbon} = 234 GPa, d = 7 μm, K_3 = 2.73 x 10^{-10} nN·m^2.

Estimation of neural probes bending force.

The force, F, to deflect a piece of three-layer longitudinal ribbons is estimated by [S5]

$$F = \frac{8eK_{1R}}{l^3}$$

Where e is the deflection of the ribbon, K_{1R} is the bending stiffness of the ribbon and l is the length of the ribbon. For the two support arms of the sensors, take $e = 10\ \mu m$, $K_{1R} = 0.54 \times 10^{-15}$ $N{\cdot}m^2$, and $l = 200\ \mu m$. $F = 2 \times 5.4\ nN = 10.8\ nN$.

© 2015 Macmillan Publishers Limited. All rights reserved

DOI: 10.1038/NMAT4427

Table S1. Key design features of a typical macroporous brain probe are summarized. All features are denoted in **Figure S2b-e.**

Key structural elements	Materials	Dimension	Thickness
i. freestanding part of the probe	SU8 and metal	6.5 mm, total length	Total ≤1 μm
ii. device region of the probe	SU8 and metal	1 mm, total width	Total ≤1 μm
iii. vertical spacing of the devices	N/A	250 μm	N/A
iv. longitudinal spacing of interconnects	N/A	50 μm	N/A
v. longitudinal interconnects	Cr/Au/Cr	5 μm, width	1.5/100/1.5 nm
	SU8	7 μm, width	400 nm/metal/400 nm
vi. transverse scrolling elements	Cr/Pd/Cr	3 μm, width	10-20/80/1.5 nm
	SU8	10 μm, width	metal/400 nm
vii. device bend-up arms	Cr/Pd/Cr	4 μm, width	1.5/80/30-50 nm
	SU8	6 μm, width	400/metal/400 nm
viii. sensor metal contact	Cr/Pd/Cr for FET	4 μm, width	1.5/50–80/1.5 nm
	Cr/Pt for electrode		1.5/100 nm
	SU8	5 μm, width	400/metal/400 nm, FET
			400 nm*, electrode

* At electrode sites, only bottom SU8 layer was defined, and the top SU8 layer was absent to expose the electrode contacts.

© 2015 Macmillan Publishers Limited. All rights reserved

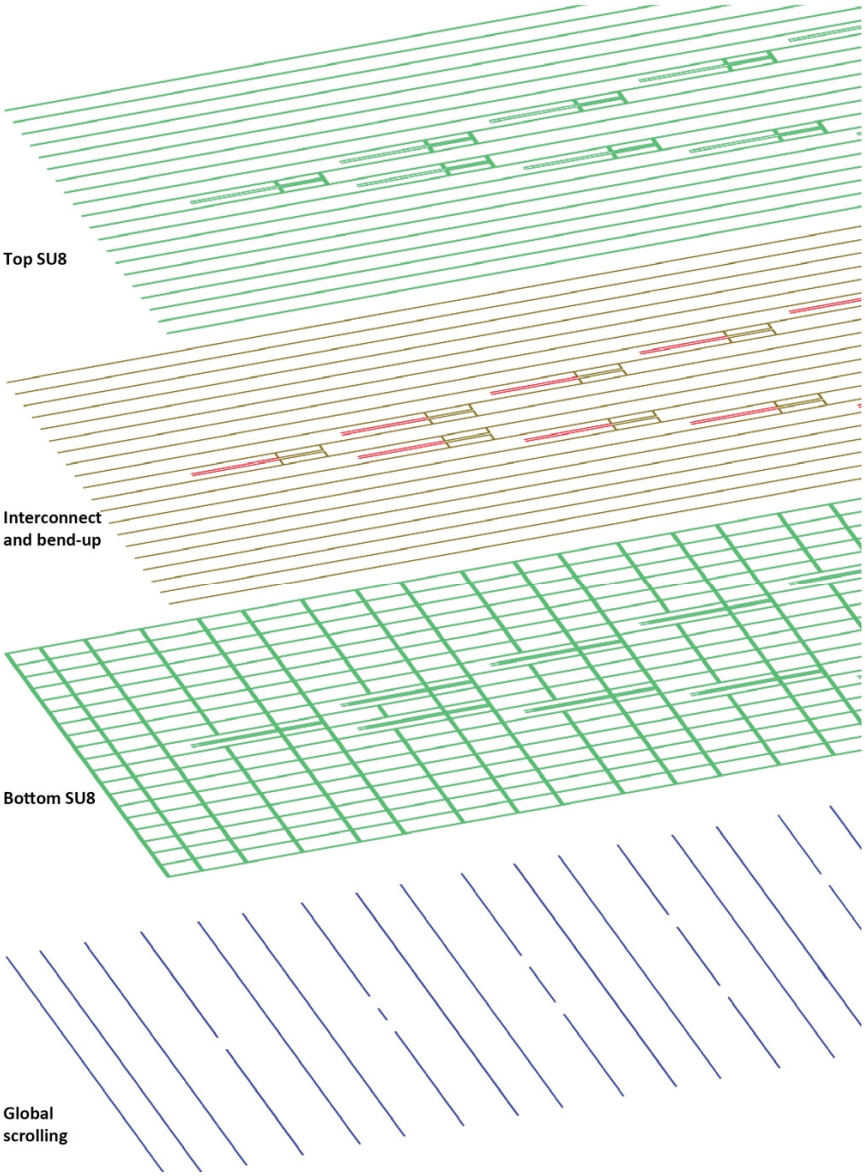

Figure S1. Major layers of a typical macroporous nanoelectronic brain probe design. Bottom-to-top correspond to the sequence defined in our fabrication flow (i.e., starting with global scrolling lines); details of fabrication steps provided in the Supplementary Methods. The purple lines in the global scrolling layer correspond to Cr/Pd/Cr metal ribbons with 10-20/80/1.5 nm thicknesses, respectively, and 3 μm widths. Green lines in Bottom and top SU-8 layers indicate 400 nm thick, 7 μm wide SU-8 ribbons. Brown lines in the Interconnects layer represents 5 μm wide Cr/Au/Cr (1.5/100/1.5 nm) interconnect lines. Red lines in the Bend-up layer arms represent 3 μm wide Cr/Pd/Cr (1.5/80/30-50 nm) metal lines.

© 2015 Macmillan Publishers Limited. All rights reserved

DOI: 10.1038/NMAT4427

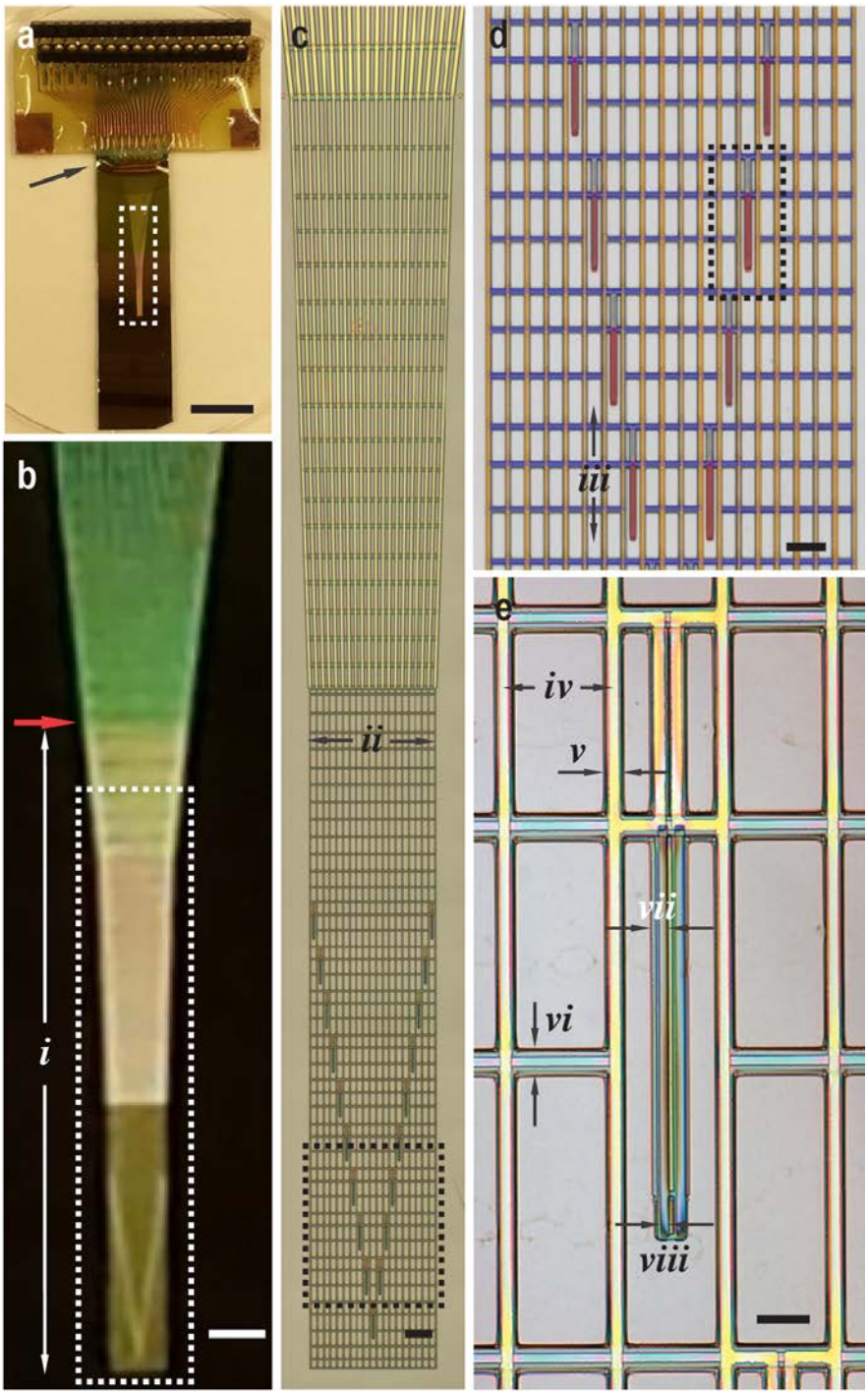

Figure S2. 2D precursor of the macroporous nanoelectronic brain probe. a, Photograph of a fully fabricated probe with attached and wire-bonded I/O connector before etching the sacrificial layer under the macroporous electronics structure. The carrier substrate (gray-black rectangle

© 2015 Macmillan Publishers Limited. All rights reserved

visible in lower-center 2/3's of image) was mounted on a custom socket/PCB connector (upper 1/3 of image), with I/O to recording instrumentation made by connections to the socket. Electrical connections between the carrier chip and PCB board were made by wire bonding (position highlighted by the black arrow). Scale bar: 1 cm. **b**, Zoom-in of the mesh electronics area of the probe from the dashed white box in **a**. The region below the red arrow is on the nickel sacrificial layer. Scale bar: 1 mm**. c**, Micrograph of the white dashed-box in **b**, which is released from the substrate following dissolution of the nickel sacrificial layer. The whole probe is designed with an open mesh structure to promote interpenetration and integration with the neural tissue. The individually-addressable sensors are located at design-specified positions in the mesh electronics; for the design shown the sensor elements define two edges of an inverted triangle (bottom 1/3 of the image). Scale bar: 200 μm. **d,** Zoomed-in view of the sensor area of the probe (black dashed-box in **c**.). The strains, which define global scrolling of the mesh electronics and bend-out of the individual sensor elements, are represented by blue and red pseudo-colored regions, respectively. The compressive strain applied in the blue regions generates positive curvature along the transverse direction of the probe, and the tensile strain applied in the red regions generates negative curvature on supporting arm of the sensor (shown in **Fig 1c**. in main text). Scale bar: 100 μm. **e,** Zoomed-in view of an individual sensor element (nanowire FET sensor, position highlighted by the black arrow), outlined by the black dashed box in **d**. The sensor is located at the tip of the supporting arms. Scale bar: 20 μm. In the panels, ***i - viii*** denote key design elements of the probe; the relevant materials and dimensions of these elements are summarized in **Table S1**.

© 2015 Macmillan Publishers Limited. All rights reserved

DOI: 10.1038/NMAT4427

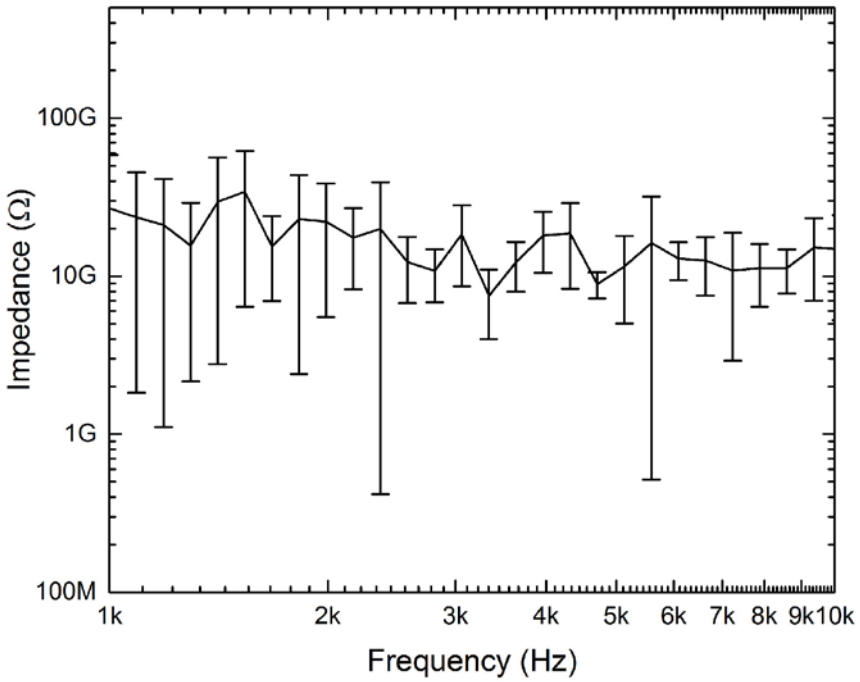

Figure S3. Frequency dependent leakage measurements of the SU8 encapsulated interconnect components. The impedance was measured between 8 pairs of interconnect metal lines in a nanowire FET probe submerged in 1X PBS, at 100 mV bias and 1 – 10 kHz. The area of each interconnect line in the 1X PBS solution was 2 mm (length) X 20 μm (width). The solid line indicates the average of the measurements and the error bars indicate ± 1-standard deviation.

© 2015 Macmillan Publishers Limited. All rights reserved

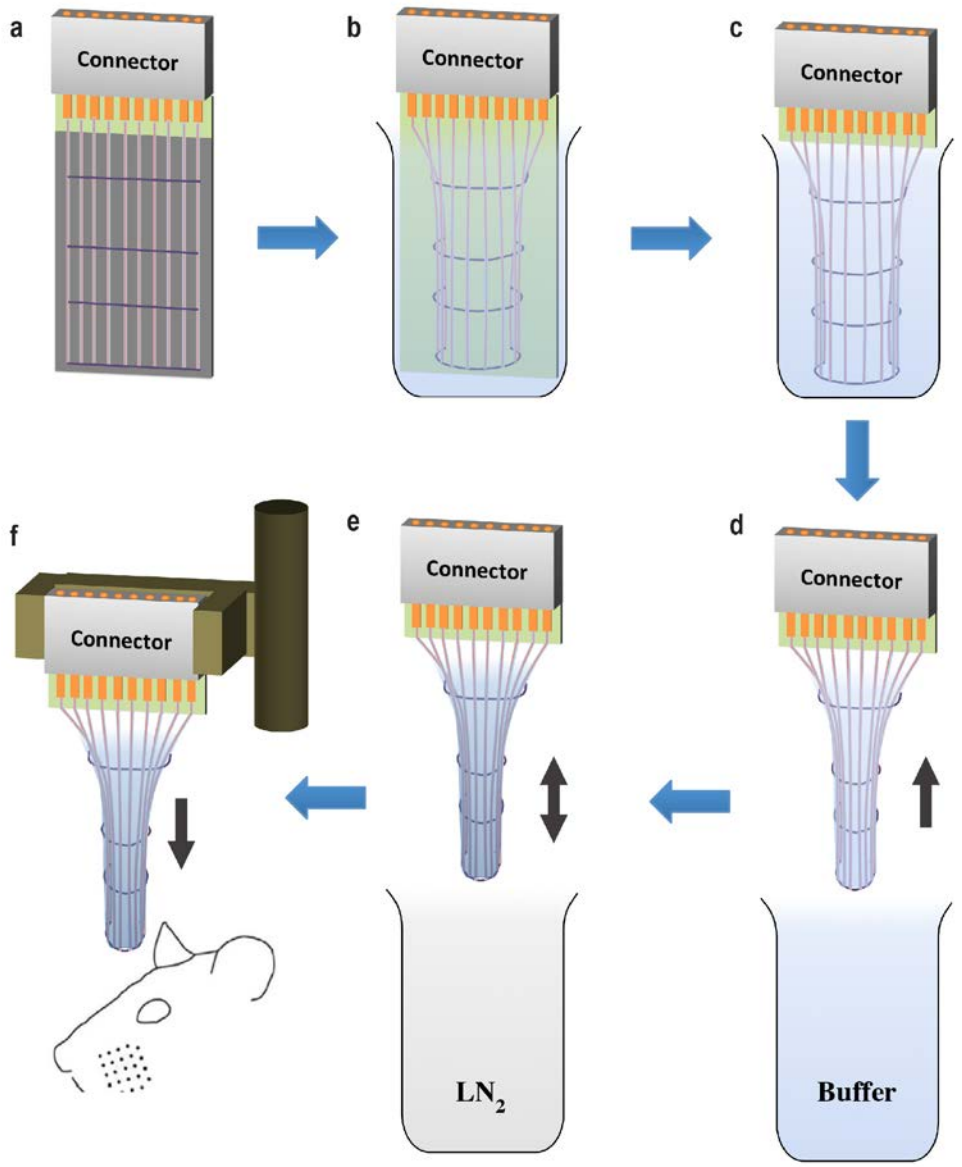

Figure S4. Schematic of probe preparation and frozen insertion. a. The fabricated macroporous neural probe on silicon carrier chip (prior to release) is attached to an I/O connector and electrical contacts are made by wire bonding. **b.** The Ni sacrificial layer is etched and the macroporous neural probe was partially released and freestanding in liquid. **c.** Excess silicon chip below the connector is trimmed off. **d.** When the device assembly is removed from the buffer solution, a small amount of buffer is trapped inside the cylindrical probe. Removal was carried out manually with a vertical speed of ca. 1-2 mm/s. **e.** The probe assembly is then slowly submerged in liquid nitrogen (LN_2) until ca. thermal equilibrium (5-10 seconds; greatly reduced LN_2 boiling). **f.** The probe is immediately mounted in a custom-holder on a linear translational stage and rapidly inserted into the brain. The insertion step was driven manually with a speed of ca. 5mm/s. The entire process should be carried out within 10 s following removal from the LN_2, with the insertion into the brain taking no more than ca. 1 second.

© 2015 Macmillan Publishers Limited. All rights reserved

DOI: 10.1038/NMAT4427

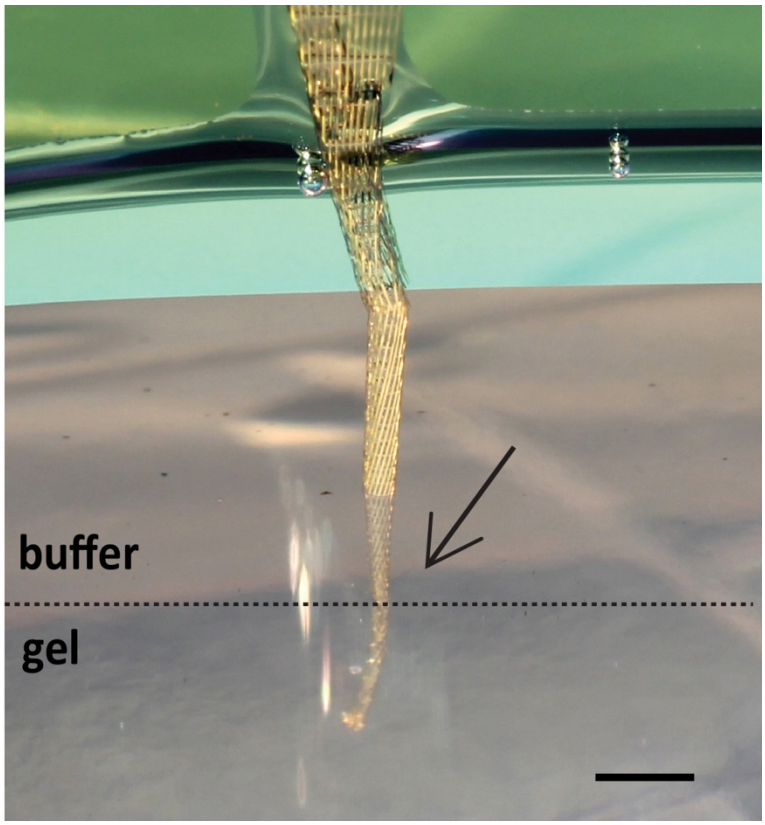

Figure S5. Probe geometry after insertion into hydrogel. Photograph showing a probe tethered to the carrier substrate following partial insertion into 0.5% agarose hydrogel with ca. 2 mm buffer solution on top. The 0.5% agarose gel provides a mechanical resistance during insertion similar to brain tissue[S6]. The insertion procedure is the same as discussed in the main text. The probe was frozen by immersion in liquid nitrogen, immediately followed by insertion, which typically took ca. 1 second. The dashed line indicates the gel / buffer boundary, and the arrow points the entry point. Scale bar: 2 mm.

© 2015 Macmillan Publishers Limited. All rights reserved

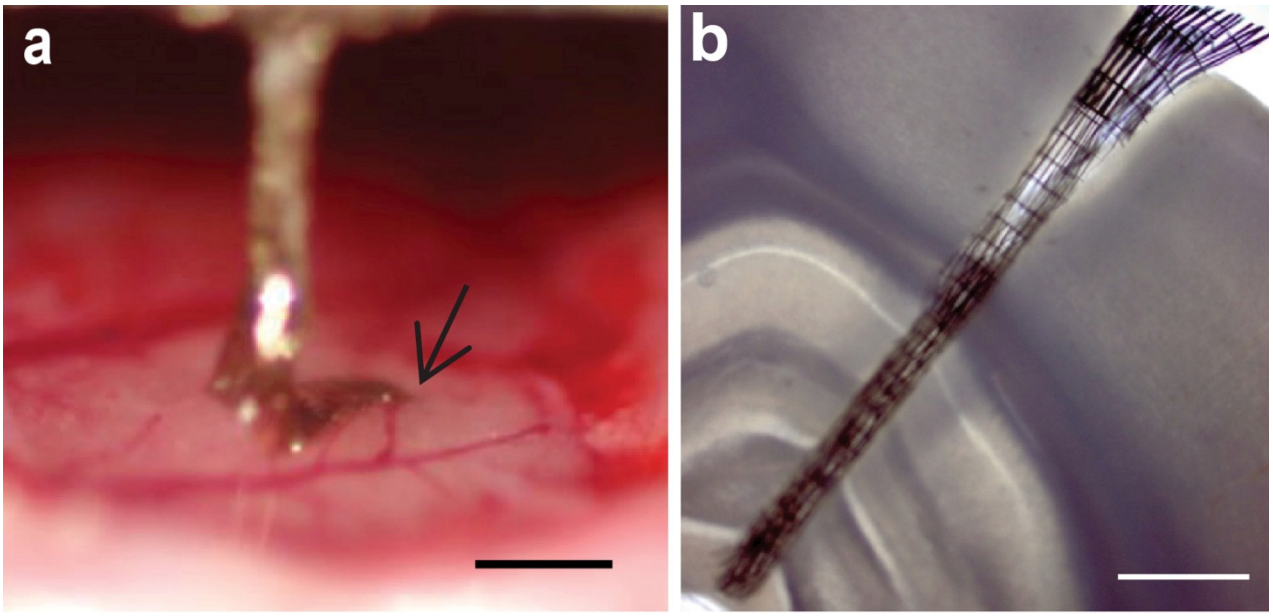

Figure S6. Probe insertion into a rat brain. a, Zoomed-in view of the implantation site in **Fig. 3a**. The arrow points the small and clean entry site into the brain. The part of the probe outside the rat brain (left of arrow) is relaxed and conformal to the brain surface due to its ultra-flexibility. Scale bar: 1 mm. **b,** Bright field image of a brain slice cut along the probe insertion direction. The brain was fixed and sliced following the procedure described in the Methods within 1 hour after implantation to reveal the probe geometry. The image shows clearly that the probe maintains a straight cylinder shape as designed, thereby yielding a predictable sensor distribution within the tissue. Scale bar: 500 μm.

© 2015 Macmillan Publishers Limited. All rights reserved

DOI: 10.1038/NMAT4427

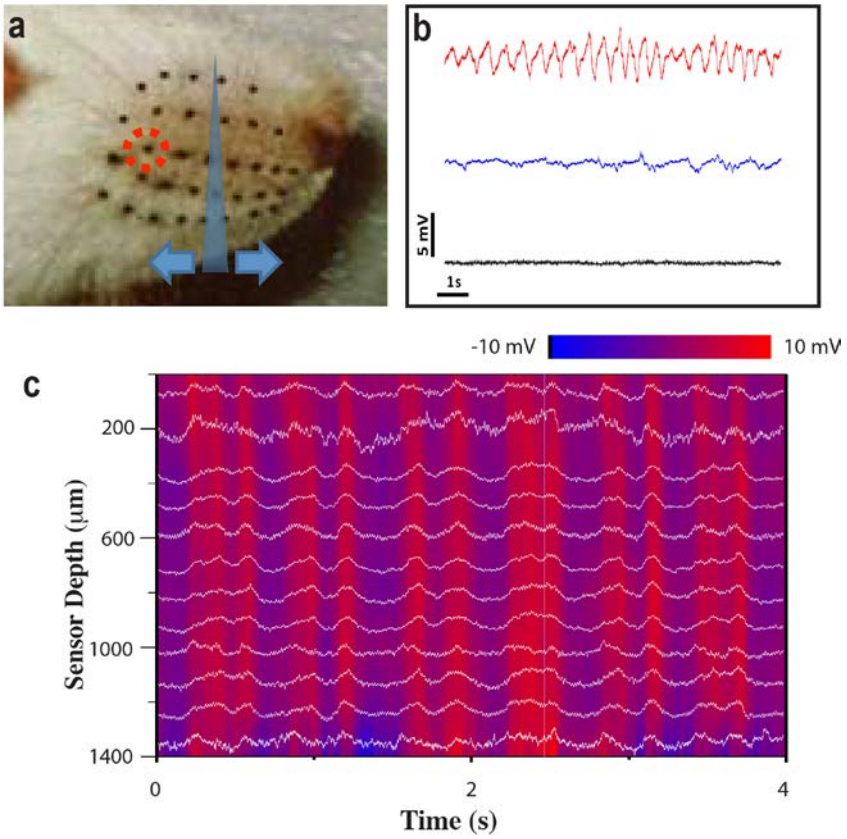

Figure S7. Identification of implanted sub-region of barrel cortex. a. A photograph of whiskers on the contralateral side of the implantation side. Mechanical stimulations were applied to all whiskers to identify the sensor close to a sub-region of barrel cortex. In this implantation and recording, element-2 (**Fig. 3b**) had the strongest response during stimulation. Subsequently, stimulation of individual whiskers on both contralateral and ipsilateral sides were carried out while simultaneous recording from the implanted mesh probe. We observed that only stimulations applied to the C1 whisker (indicated by dashed circle) on the contralateral side could elicit a strong response from element-2 of the probe. **b**, Three representative recordings from element-2. Red, while stimulating C1 whisker; blue, while stimulating the adjacent whisker C2; black, while stimulating whisker C1 after the rat was euthanized. **c,** A 4-second map of the multiplexed LFP recording from the same experiment as shown in **Fig. 3c.** The vertical axis represents the depth beneath the brain surface. The horizontal axis indicates the recording time. Colors highlight the amplitude of the recorded LFPs.

© 2015 Macmillan Publishers Limited. All rights reserved

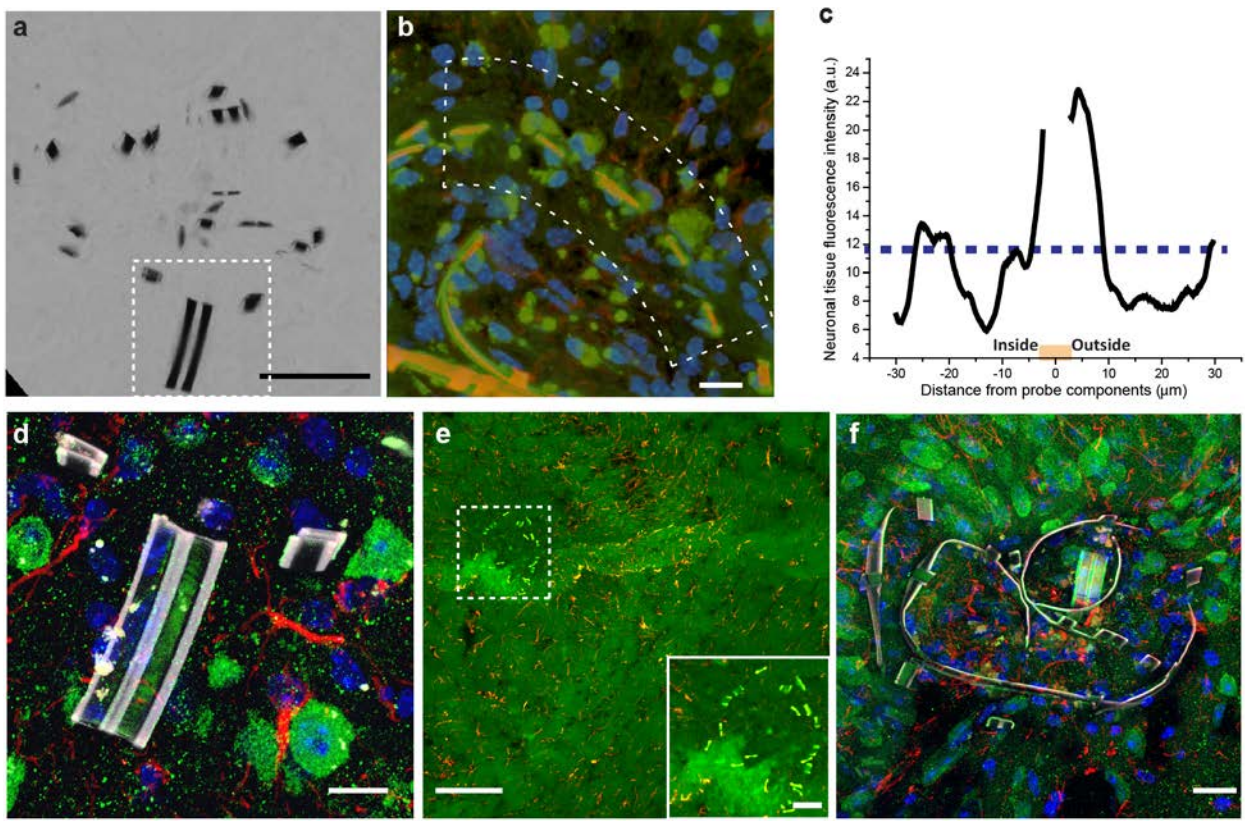

Figure S8. Histology of the probe-tissue interface. **a.** Bright field images of a 20 μm thick slice showing the interface 5 weeks post implantation. The brain tissue has interpenetrated the probe with time (compared with acute cross-section images (e.g., **Fig. 4b**). Dashed box indicates a pair of supporting arms with a sensor at the end. Scale bar: 50 μm. **b,** The reconstructed confocal micrograph of immunochemically labeled cross-section slice shown in **Fig. 4e**, where the curved dashed box here encompasses tissue both inside and outside the indicated the curved probe surface. The pseudo color-coding is as follows. Blue: nucleus stained with Hoechst; green: neurons stained with β-tubulin-III; orange: SU-8, and red: GFAP. Scale bar: 10 μm. The fluorescence intensity in the dashed area is used to analyze the affinity of neurons to probe components. **c,** The average neuron fluorescence intensity from green channel (β-tubulin-III, neuronal tissue) along the short axis of the outlined area in **b** is plotted, from inside of the probe to outside. The orange line indicates the position of probe. The blue dashed line indicates the average fluorescence intensity of the green channel in the whole image. These results demonstrate there is a higher density of neurons near the probe components, and thus suggest a

© 2015 Macmillan Publishers Limited. All rights reserved

DOI: 10.1038/NMAT4427

tendency of neurons to form tight junctions with the probe components. The tissue slices were prepared 5-weeks post implantation into the somatosensory cortex region of a mouse (Methods). **d.** Zoom-in view of a bend-up nanowire sensor in **Fig. 4c** (indicated as dashed box area in **a.**) illustrating the proximity of sensor arms and neurons as well as the intact SU-8/metal/SU-8 structure. Scale bar: 10 μm. **e.** A reconstructed confocal micrograph of immunochemically labeled cross-section from the same mouse brain and brain probe sample as used in **Fig. 4C**. Scale bar: 100 μm**. Inset:** Zoom-in view of the white boxed region. Scale bar: 20 μm. The sample was ca. 5 slices/120 μm deeper in the brain relative to Fig. 4C; the same staining and imaging methods were used for both samples. **f.** A "collapsed" probe resulting from slow implantation of the frozen probe (i.e. insertion time of the probe in the brain tissue longer > 1 s). The probe becomes randomly folded due to thawing before the insertion was completed. This result demonstrates the importance of rapid insertion of the frozen probes to maintain the designed geometry. Although the probe did not hold the designed geometry, this probe also showed tight integration with neurons, which is consistent with the macroporous ultra-flexible nature of the structure. The tissue slices were prepared 5-weeks post implantation into the somatosensory cortex region of a mouse using the same the same staining method as in in **Fig. 4C** (Methods). Scale bar: 20 μm.

© 2015 Macmillan Publishers Limited. All rights reserved

Supplementary References

S1. Patolsky, F., Zheng, G. & Lieber, C. M. Fabrication of silicon nanowire devices for ultrasensitive, label-free, real-time detection of biological and chemical species. *Nat. Protoc.* **1**, 1711-1724 (2006).

S2. Dellas, N. S., Schuh, C. J. & Mohney, S. E. Silicide formation in contacts to Si nanowires. *J Mater Sci* **47**, 6189-6205 (2012).

S3. Lee, K. N., *et al.* Stress-induced self-rolled metal/insulator bifilm microtube with micromesh walls. *J Micromech Microeng* **23** (2013).

S4. Javey, A., Nam, S., Friedman, R. S., Yan, H. & Lieber, C. M. Layer-by-layer assembly of nanowires for three-dimensional, multifunctional electronics. *Nano Lett.* **7**, 773-777 (2007).

S5. Steif, P. S. *Mechanics of materials*. Pearson: Upper Saddle River, NJ, 2012.

S6. Sharp, A. A., Ortega, A. M., Restrepo, D., Curran-Everett, D. & Gall, K. In vivo penetration mechanics and mechanical properties of mouse brain tissue at micrometer scales. *IEEE Trans. Biomed. Eng.* **56**, 45-53 (2009).

© 2015 Macmillan Publishers Limited. All rights reserved

DOI: 10.1038/NMAT4427

Supplementary Movies Captions:

Supplementary Movie 1: Withdrawal of a macroporous nanoelectronic mesh probe from aqueous buffer solution to air. As the probe moves from liquid to air, the liquid surface tension increases the global curvature to yield a straight cylinder. The movie is in real time.

Supplementary Movie 2: Variation in the geometry of the macroporous nanoelectronic mesh probe sensor arms as the probe end is withdrawn into air and then reinserted into aqueous buffer solution. The movie is in real time.

© 2015 Macmillan Publishers Limited. All rights reserved